photonics

MDPI

Communication

Scintillation and Luminescent Properties of the $(Gd,Y)_3Al_2Ga_3O_{12}$:Ce Ceramics Obtained by Compaction of Green Bodies Using Digital Light Processing 3D Printing

Lydia V. Ermakova [1,*], Valentina G. Smyslova [1], Valery V. Dubov [1], Petr V. Karpyuk [1], Petr S. Sokolov [1], Ilia Yu. Komendo [1], Aliaksei G. Bondarau [2], Vitaly A. Mechinsky [1,2] and Mikhail V. Korzhik [1,2,*]

[1] National Research Center "Kurchatov Institute", 123098 Moscow, Russia; smyslovavg@gmail.com (V.G.S.); valery_dubov@mail.ru (V.V.D.); silancedie@mail.ru (P.V.K.); sokolov-petr@yandex.ru (P.S.S.); ilia.komendo@cern.ch (I.Y.K.); vitaly.mechinsky@cern.ch (V.A.M.)

[2] Institute for Nuclear Problems, Belarusian State University, 220030 Minsk, Belarus; a.bondarev.by@gmail.com

* Correspondence: ermakova.lydiav@yandex.ru (L.V.E.); mikhail.korjik@cern.ch (M.V.K.)

Abstract: Dense and transparent ceramic samples of a $(Gd,Y)_3Al_2Ga_3O_{12}$:Ce scintillator were obtained by using stereolithography-based Digital Light Processing (DLP) 3D printing for compacting, subsequent burnout, and pressureless sintering. The effects of stoichiometric deviations and green body compaction methods (uniaxial pressing versus DLP 3D printing) on the optical, luminescent, and scintillation properties of ceramics were analyzed. An excess of Y and Gd in the composition led to an increase in transmittance and to the acceleration of the scintillation kinetics. Moreover, transparent ceramics made of 3D-printed green bodies were found to be superior in light yield to the samples, which were prepared from the same powders and densified by uniaxial pressing.

Keywords: 3D printing; ceramics; garnet oxide; light yield; luminescence; scintillation

Citation: Ermakova, L.V.; Smyslova, V.G.; Dubov, V.V.; Karpyuk, P.V.; Sokolov, P.S.; Komendo, I.Y.; Bondarau, A.G.; Mechinsky, V.A.; Korzhik, M.V. Scintillation and Luminescent Properties of the $(Gd,Y)_3Al_2Ga_3O_{12}$:Ce Ceramics Obtained by Compaction of Green Bodies Using Digital Light Processing 3D Printing. *Photonics* **2024**, *11*, 695. https://doi.org/10.3390/photonics11080695

Received: 18 June 2024
Revised: 24 July 2024
Accepted: 25 July 2024
Published: 26 July 2024

1. Introduction

Inorganic scintillator materials based on complex oxides with a garnet crystal structure (cubic, *Ia-3d*, #230), specifically $(Gd,Y)_3Al_2Ga_3O_{12}$ doped with cerium (GYAGG:Ce), are of great interest for ionizing radiation detection applications or as a promising detector in modern medical X-ray and Computed Tomography (CT) scanners due to their excellent chemical and thermal stability, high light output, good energy resolution, and relatively short photoluminescence decay [1–3]. GYAGG:Ce ceramics possess a high density of about ~6 g/cm^3, high effective atomic number [4], and good radiation hardness [1,5,6], which makes them useful for the measurement of ionizing radiation. The excellent mechanical properties [7,8] and machinability of GYAGG:Ce have also been demonstrated [8]. Another important advantage of Ce^{3+} ions in a garnet matrix is their good spectral compatibility with the sensitivity range of various semiconductor photosensors. Beyond that, in comparison to the expensive process of single-crystal growth, transparent garnet ceramic fabrication is a less time-consuming process; no precious metal tooling is used. The production process is paired with the ability to precisely modify their composition as well as size and shape [9–11]. Thus, the development of techniques to make ceramic manufacturing more cost-effective is greatly demanded.

Traditional methods of manufacturing dense advanced functional ceramics, such as cold and hot iso-static pressing [12,13] or spark plasma sintering [14], are commonly used. However, these methods allow the production of objects with simple shapes, requiring expensive molds and possessing well-known size limitations. Also, these methods require complex equipment. One of the possible ways to overcome these limitations is through 3D printing compaction of the green bodies (making the object layer by layer) [15–25].

Several studies have reported the successful fabrication of oxide ceramics with a garnet crystal structure using various 3D printing methods. Recently, we demonstrated

the use of DLP 3D printing to create the first-ever scintillation $Y_3Al_5O_{12}$:Ce (YAG:Ce) ceramics with complex shapes [15]. Later on, the same technique was employed to produce Al_2O_3/YAG:Ce^{3+} luminescent ceramics for high-flux laser lighting [16]. Transparent LuAG:Ce ceramics with a free geometric structure design for the same application were also successfully fabricated [17]. Stereolithography was also used to obtain YAG:Yb [18] and YAG [19] transparent ceramics, followed by free sintering that required the addition of sintering aids such as tetraethyl orthosilicate (TEOS) [14,18–20]. At the same time, silicon-containing sintering additives can have a negative effect on the scintillation properties of garnet oxides, reducing photoluminescence emission and light yield [11].

It is clear that such layer-by-layer polymerization methods show one of the highest printing resolutions in comparison with extrusion, for example. Although two-photon polymerization (TPP) offers even better resolution, direct printing using resin filled with inorganic material is currently not feasible due to process limitations. Transparent micrometer-sized YAG:Nd ceramics were fabricated by using a solution of metal salts that can undergo a sol–gel process and photopolymerization by two-photon printing [21]. However, the TPP method has extremely low performance and poor prospects for scaling.

Another popular 3D printing method used to produce garnet ceramics is direct ink writing (DIW), which was reported for YAG [22] and Nd:YAG [23,24] ceramic manufacturing. Unlike stereolithography, the green bodies obtained through DIW still require the use of iso-static pressing after sintering to achieve desirable high transmittance.

Here, we report for the first time a successful fabrication of GYAGG:Ce transparent ceramics in the application of DLP 3D printing for compacting the powder of a scintillator. The essential properties of the ceramics, such as photoluminescence and scintillation, were equal or superior to those measured for ceramics of the same composition obtained from the application of the traditional compacting method of uniaxial pressing.

2. Materials and Methods

2.1. Synthesis of the Initial Powders

High-purity chemical reagents, such as Gd_2O_3 (99.995%), Y_2O_3 (99.995%), AlOOH (99.998%), Ga (99.999%), and $Ce(NO_3)_3$ (99.95%), were used as raw materials to prepare nitrate solutions for synthesizing GYAGG:Ce powders of various compositions through coprecipitation [11,25,26]. The reagents were mixed in the required proportions and then diluted to obtain a total Me^+ ion concentration of ~1 mol/L. The mixture was added gradually to an ammonium hydrogen carbonate (NH_4HCO_3) solution with continuous stirring. Subsequently, the resulting precipitates were filtered, washed several times with deionizing water and isopropanol, and then calcined at a temperature of 1250 °C. Following that, the oxide powders were milled down to d_{50} ~ 2.5 μm for 60 min in a planetary ball mill PM100 (Retsch GmbH, Haan, Germany) with alumina jars and beads using isopropanol as the medium. In one case superstiochiometric additive (excess ~ 5%) of fine Y_2O_3 powder as a self-sintering aid for GYAGG:Ce was inserted during the milling process [27,28]. A combination of Gd and Y in 5% excess of the stoichiometric amount was added during the chemical synthesis stage. Table 1 provides the chemical compositions, calcining temperatures, and abbreviations of the powders.

Table 1. Garnet powders used in this study for photocurable slurry preparation.

Abbreviation	Composition	Calcining Temperature (°C)	Density (g/cm^3)
GYAGG:Ce	$Gd_{1.194}Y_{1.791}Ce_{0.015}Al_2Ga_3O_{12}$	1250	5.85
GYAGG:Ce+5%Y	$Gd_{1.194}Y_{1.88}Ce_{0.015}Al_2Ga_3O_{12}$		5.89
GYAGG:Ce+5%Y,Gd	$Gd_{1.569}Y_{1.569}Ce_{0.012}Al_2Ga_3O_{12}$		6

The phase purity of all powders and ceramics was confirmed by X-ray diffraction using a diffractometer D2 Phaser (Bruker, Billerica, MA, USA) with Cu Kα radiation, and

equipped with a LYNXEYE detector under room conditions. The Rietveld refinement of X-ray diffractions is performed using the JANA 2006 software package.

The specific surface values of the GYAGG:Ce powders were determined according to the capillary nitrogen condensation method using BET model values on a NOVA 4200e (Quantachrome Instruments, Anton Paar Group, Graz, Austria). The typical specific surface value was 4.3(1) m^2/g.

2.2. Slurry Preparation and Green Bodies Fabrication

The resin consisted of 1,6-Hexanediol diacrylate (HDDA, assay $\geq$ 80%, Sigma-Aldrich, St. Louis, MI, USA), well known for its low viscosity and high polymerization rate [15,29]. According to the supplier information, the HDDA monomer contains up to 100 ppm monomethyl ether hydroquinone (MEHQ) as an inhibitor. Based on our measurements at 25.0 °C, the dynamic and kinematic viscosities of HDDA are 6.6 mPa s and 6.5 mm^2/s, respectively.

For decreasing viscosity, commercially available phosphorous-free hyperbranched polyester-based dispersant was added with a dosage of ~2 mg/m^2 [30]. To initiate a radical polymerization reaction, a UV photoinitiator of the phosphine oxide class, 1 wt.% of HDDA, was used. The selected organic components were consistently mixed, followed by the addition of the GYAGG:Ce powders in several steps to achieve a solid load of 30–41 vol.% (70–80 wt.%).

The viscosity of the slurries was determined by conducting measurements with a Physica MCR-52 rheometer (Anton Paar, Graz, Austria) at a fixed temperature of 20.0 °C, using a parallel-plate geometry with a disk diameter of 25 mm and a gap of 0.5 mm. The range of shear rates applied during the measurements was from 1 to 200 s^{-1}. The measured viscosity and polymerization depth curves of the suspensions used in this work are given in the Supplementary Materials (Figure S1). The viscosity of the slurries increased with the increasing use of garnet powder from 0.2 Pa·s to 3.5 Pa·s at a 50 s^{-1} shear rate for 30 and 41 vol.%, respectively.

The 3D printing of green bodies was carried out using the cheap, desk-top, bottom-up and easily commercially available DLP 3D printer Photon Ultra (Anycubic, Shenzhen, China). This 3D printer uses a micro mirror array projector (Texas Instrument, Dallas, TX, USA) for the layer-by-layer controlled polymerization of a photocurable slurry through the bottom of a printing vat. The lateral resolution on the XY plane of the printer is 80 × 80 µm. The light-radiation power of the UV projector (λ = 405 nm) was measured with a UV-light meter Model 222 (G&R Labs, Santa Clara, CA, USA) and amounted to 2.5 mW/cm^2. Note that the Photon Ultra is a beginner-level 3D printer. Its brightness is approximately five to ten times lower than the typical value for professional 3D printers designed specifically for printing with high-loaded ceramic slurries [31,32].

A simple object was chosen as the printing model—a disk with a diameter of 20 mm and a thickness of 1.0 mm. For the composition GYAGG:Ce+5%Y,Gd, the dimensions for a similar model were 15 × 1 mm. A printing layer of 50 µm thickness required above 50 mJ/cm^2 total UV-light energy exposure. The layer exposure time was 70 s, due to the low photosensitivity of photocurable suspensions filled with cerium-activated garnet powders [32]. The chosen increased time ensured good adhesion between the layers due to the curing depth being set about two times higher than the layer thickness [29].

After 3D printing, the green bodies were rinsed in a laboratory ultrasonic bath several times, then the samples were dried for a few days under ambient conditions. To remove the organic binder, the fabricated green parts were continuously heated from room temperate to 550 °C in an inert atmosphere (95% Ar+5% H_2 [19]) at a rate of 0.6 °C/min. Ceramic bulk sintering was performed in a tube furnace with an oxygen flow at 1650 °C for 2 h [4]. For GYAGG:Ce+5%Y,Gd, the samples were sintered both at 1720 °C for 2 h in oxygen and at 1650 °C for 2 h in air. As well-studied comparison objects, green bodies of the same size and geometry were obtained through uniaxial pressing at 64 MPa and then sintered at the same conditions and temperature. After sintering, GYAGG:Ce ceramics were ground and polished using silicon carbide abrasive papers [4]. Additionally, to

examine the microstructure of ceramics, samples were fixed in epoxy resin, sanded down, and polished to reveal a cross section; no thermal or chemical etching was applied.

2.3. Ceramic Sample Characterization

The apparent density of the ceramic samples was measured using Archimedes' method in Lotoxane at room temperature. In all cases, the apparent density was >99%.

Ceramic microstructures were studied using a Jeol JSM-7100F (JEOL, Tokyo, Japan) scanning electron microscope (SEM). SEM images were obtained in secondary electron and backscattered electron modes. Carbon coating was used to ensure the electrical conductivity of the surface ceramic sample. The processing of the SEM images to determine the average grain sizes was carried out using ImageJ software version 1.54.

For photoluminescence (PL) and excitation spectra measurements, a Fluorat-02-Panorama spectrofluorimeter (Lumex, St. Petersburg, Russia) with a xenon lamp light source was used. The photoluminescence kinetics were studied on a FluoTime 250 luminescence spectrometer (PicoQuant, Berlin, Germany) using a pulsed LED excitation source with a wavelength of 340 nm and a pulse width of 200 ps, corresponding to the excitation of the $4f \rightarrow 5d_2$ interconfigurational transition of Ce^{3+} ions. The instrument response function was defined as 2 ns. All measurements were performed at room temperature.

The full and in-line transmittance of the samples in the visible region of the spectrum (400–700 nm) was determined on a Specord Plus spectrophotometer (Analytik Jena, Jena, Germany) equipped with an integrating sphere.

The scintillation light yield was evaluated from the photo-absorption peak positions in the amplitude spectra of γ-quanta (662 keV, ^{137}Cs) measured with an XP2020 Philips photomultiplier tube (PMT). As a reference sample, a YAG:Ce single-crystal sample with matted surfaces was used to mimic ceramic samples with a light output of 24,000 photons/MeV when excited by γ-quanta. Scintillation kinetics were measured by the delayed coincidence method on a Philips XP2020 PMT with a pulse width of 1.2 ns. The intrinsic time resolution was defined to be 2.9 ns.

3. Results and Discussion

GYAGG:Ce ceramics have a typical garnet's grain structure (Figure 1a) [10,25,26,28,33]. One can see that the superstoichiometric additive causes a notable enlargement of the average grain size, growing from 1.2 to 6.2 μm (Figure 1b). Furthermore, this additive completely eliminates any visible pores within the material due to the coalescence process.

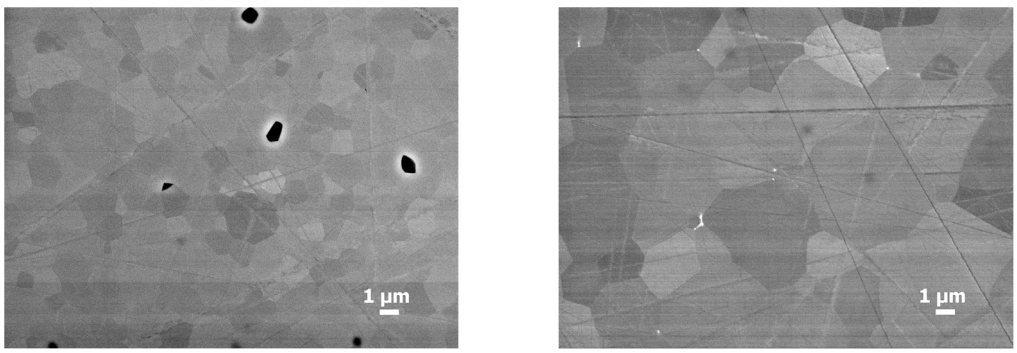

(**a**) (**b**)

Figure 1. SEM images of the cross section of (**a**) GYAGG:Ce; (**b**) GYAGG:Ce+5%Y ceramics, obtained from 3D-printed green bodies. Samples were sintered in an oxygen flow at 1650 °C for 2 h. The black areas in the left image are pores.

X-ray diffraction patterns for the initial GYAGG:Ce powder and for GYAGG:Ce ceramics are shown in the Supplementary Materials, Figure S2. Only narrow intense lines corresponding to the garnet phase are observed in the patterns. The calculated lattice

parameters for GYAGG:Ce powder and for GYAGG:Ce ceramics are a = 12.217(3) Å and a = 12.222(3) Å, respectively. The slight difference in the lattice parameter between the powder annealed at 1250 °C and the corresponding ceramic sintered at 1650 °C is associated with their different crystallinities. The solid-phase reaction to produce garnet phase only occurs completely at elevated temperatures. At the same time, the lattice parameters obtained are close to those described in the literature previously [34–37]. The calculated lattice parameter for GYAGG:Ce+5%Y ceramics is a = 12.229(2) Å. The diffraction patterns of GYAGG:Ce+5%Y ceramics contain an additional very weak line (at 30.5° 2θ), which can be attributed to the highest-intensity line of the m-$Y_4Al_2O_9$-like phase (Figure S2c). This fact is quite comparable to the results of electron microscopy (Figure 1b). One can see inclusions of small impurity grains at the junction of the garnet phase. So, it can be assumed that the optimal amount of self-sintering additive in a complex garnet-type oxide is most likely 2–3%, but 5% is an excessive amount.

Figure 2 demonstrates ceramic samples of different compositions, obtained both by uniaxial pressing and 3D printing (the initial suspension solid loading was 35 vol.%).

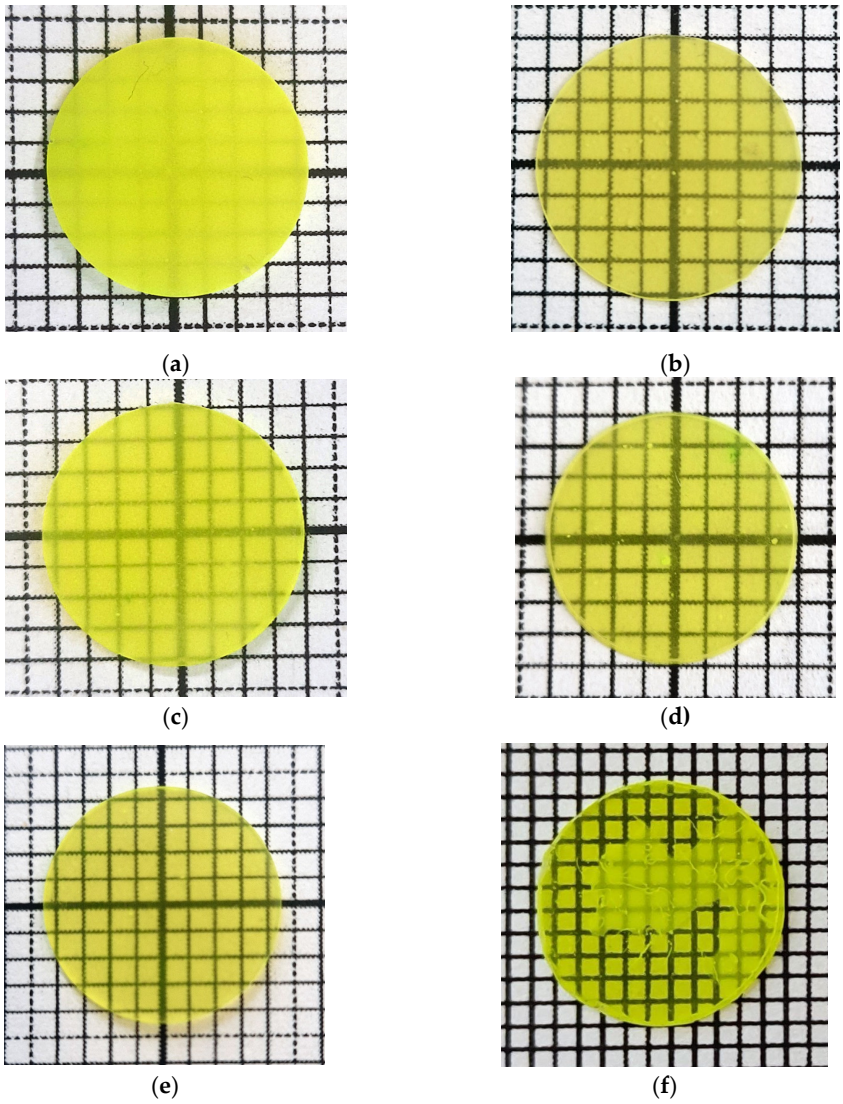

Figure 2. Optical images of ceramics: (**a**) GYAGG:Ce pressed; (**b**) GYAGG:Ce 3D; (**c**) GYAGG:Ce+5%Y pressed; (**d**) GYAGG:Ce+5%Y 3D; (**e**) GYAGG:Ce+5%Y,Gd pressed; (**f**) GYAGG:Ce+5%Y,Gd 3D. All samples were sintered for 2 h at 1650 °C in an oxygen atmosphere, except for (**e**,**f**) where the temperature was raised to 1720 °C. The sizes of the background cells are 1.5 × 1.5 mm (**a**–**e**) and 1.0 × 1.0 mm (**f**).

After sintering in an oxygen atmosphere, all disks (~1 mm thick) were semi-transparent and their visible transmittance increased with the addition of Y and Gd (Figure 2). For the GYAGG:Ce+5%Y,Gd samples, the positive impact was enhanced by raising the temperature up to 1720 °C. In general, samples obtained using photocurable slurries (Figure 2, right column) were more translucent than the samples of the same composition obtained by semi-dry uniaxial pressing (Figure 2, left column). Thus, the structure of the green bodies obtained from liquid slurries is more favorable for the formation of dense garnet ceramics, perhaps due to a better package of initial powder.

Note: carrying out the debinding process in an inert atmosphere made it possible to obtain samples without major visible defects (Figure 2). Also, the ceramic samples demonstrated transparency after high-temperature pressureless sintering in air, which increased significantly when conducting the process in an oxygen atmosphere.

Apparently, the reason for the reduced transparency of 3D-printed GYAGG:Ce ceramics sintered at temperatures sufficiently smaller than the melting point is the presence of residual pores. A small number of micron-scale pores (Figure 1a) in the cross section came from the air bubbles in the slurry mixing process, which remained in the green body after photocuring and in the ceramics after sintering. A further way to significantly improve the quality of ceramics is to increase the loading, homogenize the slurry under a vacuum, and modify the printing mode (increasing the delay time before the layer curing).

Thus, as the result of 3D printing using these simple-formula slurries, disk-shaped green bodies were obtained. This form allows for a more dependable evaluation of the key characteristics of the resulting ceramics (density and light transmission) using reliable instrumental methods.

The optical transmittance in the spectral range of scintillation of the samples obtained from the 3D-printed green bodies is depicted in Figure 3. One can see an increase in light transmission with the presence of a sintering additive. Thus, pores are the main reason for the low transparency of ceramics. The presence of trace amounts of impurity phases has a rather weak effect.

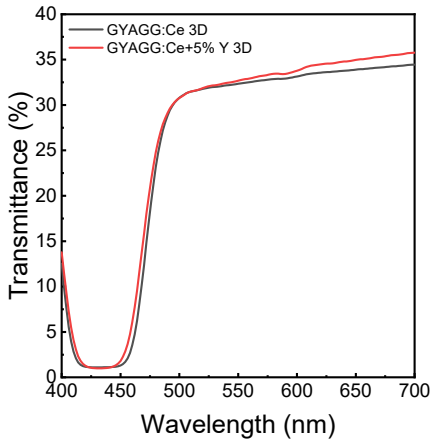

Figure 3. Transmittance of GYAGG:Ce ceramic samples of ~0.9 mm thickness for different compositions (indicated) obtained from 3D-printed green bodies.

The normalized photoluminescence (PL) and photoluminescence excitation (PLE) spectra of the ceramic samples obtained with two techniques for compacting are demonstrated in Figure 4. No difference in the shape and position of the bands was observed. The photoluminescence and photoexcited spectra of the ceramic exhibit a typical profile for Ce^{3+} ions in a garnet oxide matrix.

The green body compacting method also does not affect the photoluminescence kinetics. Table 2 lists the results of an approximation of the PL kinetics by three exponential decay components (Figure 5). The effective decay time constants **<τ>** were defined to be in the range of 50–60 ns, which is typical for garnets doped with Ce^{3+} ions [25]. When the

superstoichiometric additive includes Gd, the tail part of the kinetics shows an increase in the intensity. This effect is similar to the kinetic change observed in ternary GAGG ceramics described in [28].

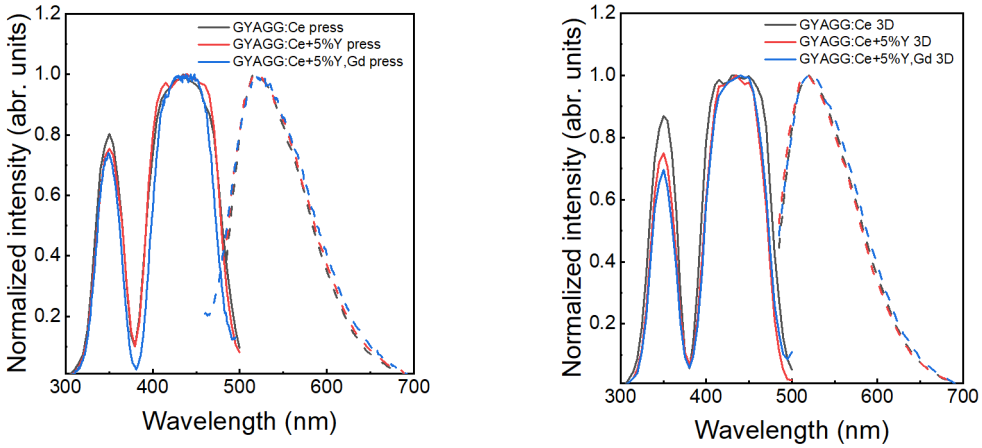

(**a**) (**b**)

Figure 4. Comparison of the room-temperature measurements and normalized luminescence (λ_{ex} = 340 nm) and excitation spectra (λ_{reg} = 520 nm) of different compositions of GYAGG:Ce ceramics, obtained using (**a**) uniaxial pressing and (**b**) 3D printing for green body compacting. Solid lines are PLE spectra; dashed lines are PL spectra.

Table 2. Decay components of the photoluminescence kinetics of GYAGG:Ce ceramics of different compositions and using the green body compacting method.

Compacting Method	Composition	τ_1 (ns)	P_1 (%)	τ_2 (ns)	P_2 (%)	τ_3 (ns)	P_3 (%)	<τ> (ns)
Uniaxial pressing	GYAGG:Ce	12.5	5.72	47.1	88.92	161	5.36	51.3
	GYAGG:Ce+5%Y	12.5	5.62	45.9	84.98	113	9.40	50.3
	GYAGG:Ce+5%Y,Gd	19.6	7.54	53.2	90.47	336	1.99	56.3
3D printing	GYAGG:Ce	17.0	14.83	50.1	79.60	287	5.57	58.4
	GYAGG:Ce+5%Y	17.9	10.20	51.7	83.51	335	6.29	66.1
	GYAGG:Ce+5%Y,Gd	15.3	9.83	47.3	78.98	162	11.19	57.0

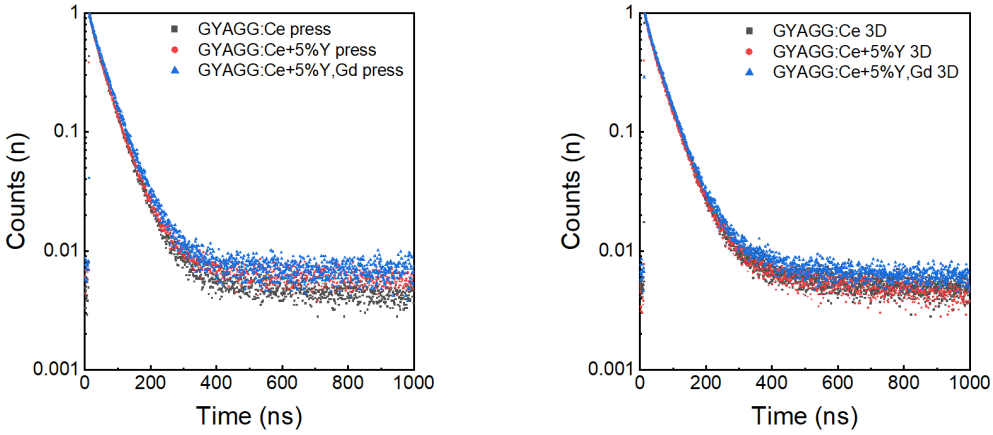

(**a**) (**b**)

Figure 5. Room-temperature PL kinetics of GYAGG:Ce ceramics of different compositions, obtained using (**a**) uniaxial pressing and (**b**) 3D printing for green body compacting.

Ceramic samples made from the green bodies obtained by different techniques and annealed at the same technological conditions have similar scintillation kinetics. However, the scintillation kinetics show variations depending on the superstoichiometric additive and ceramic sintering temperature. Two samples were evaluated for their scintillation kinetics (Figure 6). The sample made with the superstoichiometric additive possesses enlarged phosphorescence, as seen from the increased number of photons detected prior to the kinetics curve. Table 3 depicts the results of an approximation by three exponential decay components of the scintillation kinetics measured at room temperature. The application of the superstoichiometric additive led to an increase in the fraction of the slowest component, but a shortening of the effective decay time was also evident. We believe that the introduction of a superstoichiometric self-sintered additive together with 20 ppm of MgO can accelerate the kinetics of PL and scintillation [9].

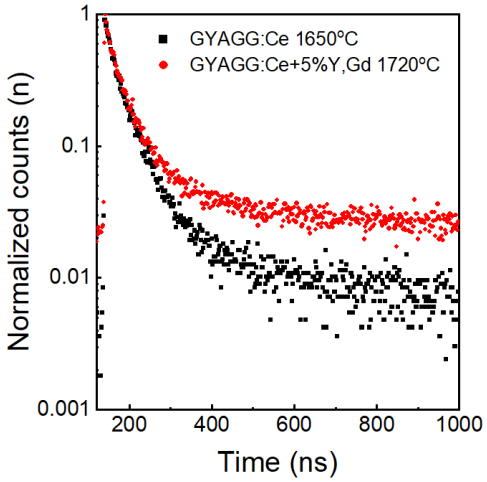

Figure 6. Room-temperature scintillation kinetics of GYAGG:Ce ceramics depending on the initial powder composition and sintering temperature.

Table 3. Decay components of the scintillation kinetics of GYAGG:Ce ceramics of different compositions.

Composition	τ_1 (ns)	P_1 (%)	τ_2 (ns)	P_2 (%)	τ_3 (ns)	P_3 (%)	τ (ns)
GYAGG:Ce	14.3	13	47.5	68.8	310	18.2	91.0
GYAGG:Ce+5%Y,Gd	11.6	8.4	41.4	63.7	173	27.9	75.6

The same samples were evaluated for LY at room temperature. Figure 7 depicts the pulse height spectra of the reference YAG:Ce and the samples GYAGG:Ce and GYAGG:Ce+5%Y,Gd. A difference in the LY between two samples is caused by different optical transmissions, which affect the collection of the scintillation light when measured. The light yield of the ceramic samples was evaluated to be 43,000–46,000 photons/MeV, which correlates rather well with the results of [25].

GYAGG:Ce single crystals have a scintillation light output of 52,000 photons/MeV. The ceramics obtained in this work by uniaxial pressing have a slightly lower light output, which is explained by their worse light transmission, which needs to be improved. Also, the scintillation kinetics of ceramic samples contain slow components that are absent in single crystals [9]. Their presence may be due to the incomplete removal of phosphorus-containing components [30], as well as the absence of magnesium or/and titanium co-doping in the composition [9].

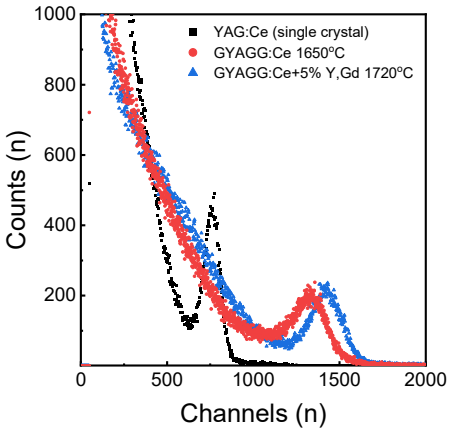

Figure 7. Pulse height spectra for GYAGG:Ce ceramic samples and reference YAG:Ce single crystal measured under γ-radiation.

4. Conclusions

Stereolithographic-based low-cost DLP 3D printing technology allows for the production of bulk GYAGG scintillation ceramics. To minimize defects in the ceramics, it is better to burn out the organic binder in an inert atmosphere.

The photoluminescent and scintillation properties of the ceramic samples obtained from the green bodies prepared by 3D printing and uniaxial pressing were practically similar. However, they were affected by the superstoichiometric additive or sintering temperature. The Gd additive resulted in a slight rise in the intensity of the kinetics' tail part. An increased amount of Y led to the enlargement of the average grain size and eliminated pores. Furthermore, applying these superstoichiometric additives led to an increase in the fraction of the slowest component, accompanied by a reduction in the effective decay time.

Supplementary Materials: The following supporting information can be downloaded at: https://www.mdpi.com/article/10.3390/photonics11080695/s1, Figure S1: Dependence of viscosity on shear rate for photocurable suspensions at 20.0 °C with different solid loadings (a); approximated cure depth curve (b); Figure S2: X-ray diffraction patterns of GYAGG:Ce initial powder and ceramics.

Author Contributions: Conceptualization, M.V.K. and P.S.S.; methodology, P.V.K., V.A.M. and A.G.B.; validation, P.V.K., M.V.K. and I.Y.K.; formal analysis, V.A.M.; investigation, P.V.K., V.V.D., V.G.S., V.A.M. and A.G.B.; resources, I.Y.K.; data curation, M.V.K.; writing—original draft preparation, L.V.E.; writing—review and editing, P.S.S., P.V.K. and M.V.K.; visualization, L.V.E.; supervision, M.V.K. and I.Y.K.; project administration, P.S.S.; funding acquisition, M.V.K. All authors have read and agreed to the published version of the manuscript.

Funding: Powder synthesis, slurry preparation, 3D printing, ceramic sintering, and optical characteristics measurements were performed with the support of the grant of the Russian Science Foundation No. 22-13-00172, https://rscf.ru/en/project/22-13-00172/ in NRC "Kurchatov institute".

Institutional Review Board Statement: Not applicable.

Informed Consent Statement: Not applicable.

Data Availability Statement: Data are contained within the article and Supplementary Materials.

Acknowledgments: The authors are very grateful to Stanislav Salykin and Ruslan Uzbekov for the dynamic and kinematic viscosity measurements of the initial acrylate monomers, respectively. The authors thank Sergey Fedorchenko for measuring the viscosity of the photocurable suspensions. The authors also express their gratitude to Rasim Saifutyarov for providing SEM images of the ceramic samples. The scintillation properties of the produced ceramic materials were measured at the Institute for Nuclear Problems of Belarusian State University. The analytical studies of GYAGG:Ce powders were carried out using X-ray diffraction and BET techniques on the equipment of the Research Chemical and Analytical Center NRC "Kurchatov institute" Shared Research Facilities.

Conflicts of Interest: The authors declare no conflicts of interest.

References

1. Jarrell, J.T.; Cherepy, N.J.; Seeley, Z.M.; Murphy, J.W.; Swanberg, E.L.; Voss, L.F.; Frye, C.D.; Stoyer, M.A.; Henderson, R.A.; O'Neal, S.P. Beta Radiation Hardness of GYGAG (Ce) Transparent Ceramic Scintillators. *IEEE Trans. Nucl. Sci.* **2022**, *69*, 938–941. [CrossRef]
2. Chen, X.; Hu, Z.; Feng, Y.; Liu, X.; Chen, H.; Shi, Y.; Kucerkova, R.; Beitlerova, A.; Nikl, M.; Li, J. Luminescence and Scintillation Characteristics of Cerium Doped $Gd_2YGa_3Al_2O_{12}$ Ceramics. *Opt. Mater.* **2019**, *90*, 20–25. [CrossRef]
3. Luo, Z.; Zhuang, Y.; Li, W.; Du, Y.; Sun, J.; Liu, Z.; Wu, Y.; Jiang, H.; Jiang, J. A new promising new choice for modern medical CT scanners: Cerium-doped gadolinium yttrium gallium aluminum garnet ceramic scintillator. *Appl. Mater. Today* **2023**, *35*, 101986. [CrossRef]
4. Seeley, Z.M.; Cherepy, N.J.; Payne, S.A. Homogeneity of Gd-Based Garnet Transparent Ceramic Scintillators for Gamma Spectroscopy. *J. Cryst. Growth* **2013**, *379*, 79–83. [CrossRef]
5. Kasimova, V.M.; Kozlova, N.S.; Buzanov, O.A.; Zabelina, E.V.; Lagov, P.B.; Pavlov, Y.S. Effect of Electron Irradiation on the Optical Properties of Gadolinium-Aluminum-Gallium Garnet Crystals. *J. Surf. Investig. X-ray Synchrotron Neutron Tech.* **2021**, *15*, 1259–1263. [CrossRef]
6. Kasimova, V.M.; Kozlova, N.S.; Zabelina, E.V.; Buzanov, O.A.; Lagov, P.B.; Pavlov, Y.S.; Kulevoy, T.V.; Stolbunov, V.S. Effect of Proton Irradiation on the Optical Properties and Defect Formation in $Gd_3Al_xGa_{5-x}O_{12}$ (x = 2, 3) Crystals. *J. Surf. Investig. X-ray Synchrotron Neutron Tech.* **2021**, *18*, 58–62. [CrossRef]
7. Kasimova, V.M.; Kozlova, N.S.; Buzanov, O.A.; Zabelina, E.V.; Targonskii, A.V.; Rogachev, A.V. Effect of Partial Substitution of Aluminium for Gallium on the Properties of Gadolinium Aluminum Gallium Garnet Single Crystals. *Inorg. Mat.* **2022**, *58*, 288–294. [CrossRef]
8. Qiu, X.; Luo, Z.; Zhang, J.; Jiang, H.; Jiang, J. Mechanical Properties and Machinability of GYGAG: Ce Ceramic Scintillators. *Ceram. Int.* **2020**, *46*, 4550–4555. [CrossRef]
9. Korzhik, M.; Alenkov, V.; Buzanov, O.; Dosovitskiy, G.; Fedorov, A.; Kozlov, D.; Mechinsky, V.; Nargelas, S.; Tamulaitis, G.; Vaitkevičius, A. Engineering of a New Single-Crystal Multi-Ionic Fast and High-Light-Yield Scintillation Material $(Gd_{0.5}–Y_{0.5})_3Al_2Ga_3O_{12}$:Ce, Mg. *CrystEngComm* **2020**, *22*, 2502–2506. [CrossRef]
10. Zhu, D.; Nikl, M.; Chewpraditkul, W.; Li, J. Development and Prospects of Garnet Ceramic Scintillators: A Review. *J. Adv. Ceram.* **2022**, *11*, 1825–1848. [CrossRef]
11. Karpyuk, P.V.; Dosovitskiy, G.A.; Kuznetsova, D.E.; Gordienko, E.V.; Fedorov, A.A.; Mechinsky, V.A.; Dosovitskiy, A.E.; Korzhik, M.V. Ceramic Scintillation Materials—Approaches, Challenges and Possibilities. In *Engineering of Scintillation Materials and Radiation Technologies: Selected Articles of ISMART2018 6*; Springer: Berlin/Heidelberg, Germany, 2019; pp. 57–74. [CrossRef]
12. Chen, X.; Qin, H.; Zhang, Y.; Jiang, J.; Jiang, H. Highly Transparent ZrO_2-Doped $(Ce, Gd)_3Al_3Ga_2O_{12}$ Ceramics Prepared via Oxygen Sintering. *J. Eur. Ceram. Soc.* **2015**, *35*, 3879–3883. [CrossRef]
13. Cheng, S.; Zou, S.; Wang, Z.; Ling, L.; Zeng, X.; Qiu, P.; Sun, D.; He, X. Fabrication and Magneto-Optic Property of Infrared Transparent Gadolinium Iron Garnet (GdIG) Ceramics by Hot-Press Sintering Process. *J. Eur. Ceram. Soc.* **2024**, *44*, 3869–3876. [CrossRef]
14. Zhang, G.; Carloni, D.; Wu, Y. Ultraviolet Emission Transparent Gd: YAG Ceramics Processed by Solid-state Reaction Spark Plasma Sintering. *J. Am. Ceram. Soc.* **2020**, *103*, 839–848. [CrossRef]
15. Dosovitskiy, G.A.; Karpyuk, P.V.; Evdokimov, P.V.; Kuznetsova, D.E.; Mechinsky, V.A.; Borisevich, A.E.; Fedorov, A.A.; Putlayev, V.I.; Dosovitskiy, A.E.; Korjik, M.V. First 3D-Printed Complex Inorganic Polycrystalline Scintillator. *CrystEngComm* **2017**, *19*, 4260–4264. [CrossRef]
16. Hu, S.; Liu, Y.; Zhang, Y.; Xue, Z.; Wang, Z.; Zhou, G.; Lu, C.; Li, H.; Wang, S. 3D Printed Ceramic Phosphor and the Photoluminescence Property under Blue Laser Excitation. *J. Eur. Ceram. Soc.* **2019**, *39*, 2731–2738. [CrossRef]
17. Li, B.; Wang, S.; Chen, J.; Li, Z.; Shan, W.; Wang, X.; Jiang, B.; He, J.; Zhang, L. 3D Printing of LuAG: Ce Transparent Ceramics for Laser-Driven Lighting. *Ceram. Int.* **2023**, *49*, 38708–38716. [CrossRef]
18. Hostaša, J.; Schwentenwein, M.; Toci, G.; Esposito, L.; Brouczek, D.; Piancastelli, A.; Pirri, A.; Patrizi, B.; Vannini, M.; Biasini, V. Transparent Laser Ceramics by Stereolithography. *Scr. Mater.* **2020**, *187*, 194–196. [CrossRef]
19. Shen, Y.; Sun, Y.; Jin, B.; Li, M.; Xing, B.; Zhao, Z. Effect of debinding and sintering profile on the optical properties of DLP-3D printed YAG transparent ceramic. *Ceram. Int.* **2022**, *48*, 21134–211140. [CrossRef]
20. Mori, M.; Xu, J.; Okada, G.; Yanagida, T.; Ueda, J.; Tanabe, S. Comparative Study of Optical and Scintillation Properties of Ce: YAGG, Ce: GAGG and Ce: LuAGG Transparent Ceramics. *J. Ceram. Soc. Jpn.* **2016**, *124*, 569–573. [CrossRef]
21. Cooperstein, I.; Indukuri, S.R.K.C.; Bouketov, A.; Levy, U.; Magdassi, S. 3D Printing of Micrometer-sized Transparent Ceramics with On-demand Optical-gain Properties. *Adv. Mater.* **2020**, *32*, 2001675. [CrossRef] [PubMed]
22. Chen, J.; Ji, H.; Zhang, J.; Wang, S.; Liu, Y. Fabrication of YAG Ceramic Tube by UV-Assisted Direct Ink Writing. *Ceram. Int.* **2022**, *48*, 19703–19708. [CrossRef]
23. Seeley, Z.; Yee, T.; Cherepy, N.; Drobshoff, A.; Herrera, O.; Ryerson, R.; Payne, S.A. 3D Printed Transparent Ceramic YAG Laser Rods: Matching the Core-Clad Refractive Index. *Opt. Mater.* **2020**, *107*, 110121. [CrossRef]

24. Jones, I.K.; Seeley, Z.M.; Cherepy, N.J.; Duoss, E.B.; Payne, S.A. Direct Ink Write Fabrication of Transparent Ceramic Gain Media. *Opt. Mater.* **2018**, *75*, 19–25. [CrossRef]
25. Chen, X.; Liu, X.; Feng, Y.; Li, X.; Chen, H.; Xie, T.; Kou, H.; Kučerková, R.; Beitlerová, A.; Mihóková, E.; et al. Microstructure evolution in two-step-sintering process toward transparent Ce:$(Y,Gd)_3(Ga,Al)_5O_{12}$ scintillation ceramics. *J. Alloys Compd.* **2020**, *846*, 156377. [CrossRef]
26. Dubov, V.; Gogoleva, M.; Saifutyarov, R.; Kucherov, O.; Korzhik, M.; Kuznetsova, D.; Komendo, I.; Sokolov, P. Micro-Nonuniformity of the Luminescence Parameters in Compositionally Disordered GYAGG: Ce Ceramics. *Photonics* **2023**, *10*, 54. [CrossRef]
27. Zhu, D.; Wu, L.; Beitlerova, A.; Kucerkova, R.; Chewpraditkul, W.; Nikl, M.; Li, J. Compositional regulation of multi-component GYGAG:Ce scintillation ceramics: Self-sintering-aid effect and afterglow suppression. *J. Adv. Ceram.* **2023**, *12*, 1919–1929. [CrossRef]
28. Retivov, V.; Dubov, V.; Kuznetsova, D.; Ismagulov, A.; Korzhik, M. Gd^{3+} Content Optimization for Mastering High Light Yield and Fast $Gd_xAl_2Ga_3O_{12}$: Ce^{3+} Scintillation Ceramics. *J. Rare Earths* **2023**, *41*, 1911–1918. [CrossRef]
29. Halloran, J.W. Ceramic Stereolithography: Additive Manufacturing for Ceramics by Photopolymerization. *Annu. Rev. Mater. Res.* **2016**, *46*, 19–40. [CrossRef]
30. Ermakova, L.V.; Smyslova, V.G.; Dubov, V.V.; Kuznetsova, D.E.; Malozovskaya, M.S.; Saifutyarov, R.R.; Karpyuk, P.V.; Sokolov, P.S.; Komendo, I.Y.; Bondarau, A.G.; et al. Effect of a Phosphorus Additive on Luminescent and Scintillation Properties of Ceramics GYAGG:Ce. *Ceramics* **2023**, *6*, 1478–1489. [CrossRef]
31. Thakur, T.; Carretta, M.; Komissarenko, D.; Blugan, G. Advancements in DLP 3D printing: High strength alumina toughened zirconia ceramics for biomedical applications. *Open Ceram.* **2024**, *18*, 100601. [CrossRef]
32. Ermakova, L.V.; Dubov, V.V.; Saifutyarov, R.R.; Kuznetsova, D.E.; Malozovskaya, M.S.; Karpyuk, P.V.; Dosovitskiy, G.A.; Sokolov, P.S. Influence of Luminescent Properties of Powders on the Fabrication of Scintillation Ceramics by Stereolithography 3D Printing. *Ceramics* **2023**, *6*, 43–57. [CrossRef]
33. Zhu, Q.-Q.; Li, S.; Yuan, Q.; Zhang, H.; Wang, L. Transparent YAG: Ce Ceramic with Designed Low Light Scattering for High-Power Blue LED and LD Applications. *J. Eur. Ceram. Soc.* **2021**, *41*, 735–740. [CrossRef]
34. Seeley, Z.M.; Cherepy, N.J.; Payne, S.A. Expanded phase stability of Gd-based garnet transparent ceramic scintillators. *J. Mater. Res.* **2014**, *29*, 2332–2337. [CrossRef]
35. Hamilton, A.S.; Lampronti, G.I.; Rowley, S.E.; Dutton, S.E. Enhancement of the magnetocaloric effect driven by changes in the crystal structure of Al-doped GGG, $Gd_3Ga_{5-x}Al_xO_{12}$ ($0 \leq x \leq 5$). *J. Phys. Condens. Matter* **2014**, *26*, 116001. [CrossRef] [PubMed]
36. Spassky, D.; Kozlova, N.; Zabelina, E.; Kasimova, V.; Krutyak, N.; Ukhanova, A.; Morozov, V.A.; Morozov, A.V.; Buzanov, O.; Chernenko, K.; et al. Influence of the Sc Cation Substituent on the Structural Properties and Energy Transfer Processes in GAGG:Ce Crystals. *CrystEngComm* **2020**, *22*, 2621–2631. [CrossRef]
37. Nakatsuka, A.; Yoshiasa, A.; Yamanaka, T. Cation distribution and crystal chemistry of $Y_3Al_{5-x}Ga_xO_{12}$ ($0 \leq x \leq 5$) garnet solid solutions. *Acta Crystallogr. Sect. B Struct. Sci.* **1999**, *55*, 266–272. [CrossRef] [PubMed]